Exploring the effects of speed and scale on a ship's form factor using CFD

Momchil Terziev [a], [*], Tahsin Tezdogan [b], Yigit Kemal Demirel [b], Diego Villa [c], Simon Mizzi [d], Atilla Incecik [a]

[a] Faculty of Engineering, University of Strathclyde, Glasgow, UK
[b] Department of Naval Architecture, Ocean and Marine Engineering, University of Strathclyde, Glasgow, UK
[c] Department of Electric, Electronic and Telecommunication Engineering and Naval Architecture (DITEN), University of Genoa, Italy
[d] Faculty of Engineering, University of Malta, Msida, Malta

ARTICLE INFO

ABSTRACT

The problem of predicting a ship's form factor and associated scale effects has been subject to many investigations in recent years. In this study, an attempt is made to investigate whether the form factor is influenced by a change in the ship's speed by numerically modelling a geosim series of the KCS hull form by means of a RANS solver. The turbulence dependence of the problem is also studied by altering the closure model among three widely used approaches (the $k\text{-}\omega$, $k\text{-}\omega$ SST, and $k\text{-}\varepsilon$ models). The results show that at very low speeds (Froude numbers in the range of 0.02–0.06) the numerical model predicts changes in the form factor of a ship between 10% and 20%, depending on the turbulence model and scale factor choices. As the speed is increased further, the form factor exhibits little change, usually in the range of 1% or less. Simulations where the Reynolds number is changed by approximately two orders of magnitude, achieved by altering the value of viscosity, confirmed that the form factor can be considered Froude-dependent only for low speeds, predicting essentially identical values when high speed cases are considered.

1. Introduction

An integral problem within the field of naval architecture is the prediction of the force required to maintain a ship's constant velocity in a calm sea. Early attempts to provide solutions to this problem were made by Euler and Newton (Gotman, 2007). However, the contemporary ideas in ship resistance prediction originate from the work of Froude (1874). In his seminal study, Froude suggested that ship resistance may be split into constituent components, which can be estimated separately and later combined to give the total value. Specifically, the most influential idea stemming from his work relates to the fact that a ship's resistance may be expressed as the sum of the resistance experienced by an equivalent flat plate, and a residuary component.

Froude's approach clearly requires the knowledge of the residual component. The estimation of this component is a non-trivial task since it contains both viscous pressure and wave resistance effects. For this reason, the currently accepted norm in the field, endorsed by the International Towing Tank Conference (ITTC), involves the estimation of a form factor $(1+k)$. This is used as a multiplicative factor to the frictional resistance. In this case, the remainder is the wave resistance, which may be estimated, for instance, by potential methods (Gotman, 2002; Havelock, 1908; Tuck and Lazauskas, 2008). Therefore, provided one has knowledge of the form factor, a suitable relation expressing the frictional resistance, and an estimate of the wave resistance, it is possible to predict the total resistance at any speed and scale factor (also known as extrapolation). It should also be mentioned that typically, a correlation allowance is added to the total to account for any discrepancies, biases, or scale effects.

To obtain a useful approximation of the total resistance of a ship, a scaled down version of the hull is produced and tested in a towing tank. This test provides the naval architect with the form factor by towing the hull at a very low speed where wave resistance is assumed negligible, also known as the Prohaska test. However, in practice, many testing facilities rely on large databases of model

* Corresponding author.
E-mail address: momchil.terziev@strath.ac.uk (M. Terziev).
Peer review under responsibility of The Society of Naval Architects of Korea.

tests and sea trial data. In other words, experimental facilities tend to rely on experience-based approaches, rather than the scientific norm.

The currently accepted practice has also endured substantive criticism by the academic community largely due to the required assumptions. Namely, the form factor is Froude and Reynolds number independent, while the wave resistance coefficient, following Froude similarity, is constant at all scales for a given speed. However, it is only possible to satisfy either Froude similarity *or* Reynolds similarity experimentally. The former, being the preferred choice for all experimental facilities results in several orders of magnitude Reynolds number discrepancy (typically $\mathcal{O}(10^6)-\mathcal{O}(10^9)$) between the model and full-scale ship.

For the reasons illustrated previously, many researchers have focused on the effect of the aforementioned dissimilarity in Reynolds number and the potential scale effects stemming from it (Dogrul et al., 2020; Kouh et al., 2009; Lee et al., 2018; Raven et al., 2008; Terziev et al., 2019a; Xiao et al., 2018). However, few studies have focused on the effect of varying Froude number on the form factor, which is what the present study aims to address. This work will therefore seek to elucidate such effects with the aim of understanding the nature of the form factor of a ship. One may justifiably expect that a scale effect would be observed when changing the Froude number since the ship speed has been changed, thereby affecting the Reynolds number. Nevertheless, it is yet unknown what importance the Froude number itself has in the observed scale effect of the form factor.

This study aims to investigate possible Froude number dependencies on a ship's form factor by the use of Computational Fluid Dynamics (CFD). This method has emerged as a popular supplement to experimentation due to its ability to handle complex three-dimensional, fully nonlinear viscous flows. As a case study, the well-known KCS ship is adopted at a wide range of Reynolds and Froude numbers. Model and full-scale simulations were performed using double body simulations, i.e. the free surface was replaced by a non-deforming symmetry plane. This is done to eliminate the wave component of ship resistance and allow the direct computation of the form factor. All simulations were performed within the commercially available Reynolds averaged Navier-Stokes (RANS) solver, Star-CCM+, version 14.02.12. To explore the influence of turbulence modelling, the closure strategy was varied using three widely used approaches: the *k-ω* model (Wilcox, 2008), the realizable *k-ε* model (Rodi, 1991; Shih et al., 1995), and the *k-ω SST* model (Menter, 1994). These modelling approaches for turbulent flows account for the vast majority of computational hydrodynamics research (Terziev et al., 2019b).

The remainder of this work is organised as follows. Section 2 is dedicated to a brief summary of the relevant contributions to the field, with emphasis on studies featuring the CFD approach. Section 3 details the case study, which is followed by the numerical set up, given in section 4. Subsequently, an estimate of the numerical uncertainty is given. Finally, the results and findings are given in section 5, whereas conclusions are given in section 6.

2. Background

Notwithstanding the previously examined constraints, imposed as part of the form factor's definition, the ITTC extrapolation procedure has merit. Other than Froude's approach, which relies on many of the same arguments, at present, the ITTC'78 approach is the only engineering scaling law available to the naval architect (ITTC, 2017). Moreover, the correlation allowance is thought to absorb many of the deficiencies. Having been calibrated specifically for the use in conjunction with the ITTC correlation line (Eq. (1)),

the analyst can have an indication of the expected frictional resistance coefficient.

$$C_{F,ITTC} = \frac{0.075}{(\log_{10} Re - 2)^2} \tag{1}$$

where Re is the Reynolds number, and $C_{F,ITTC}$ is the frictional resistance coefficient, obtained via the ITTC correlation line.

However, the extrapolation procedure is not fully consistent with the physical phenomena underpinning ship resistance. Boundary layer physics suggest that at full-scale, the ship's boundary layer is thinner than at model-scale in relative terms. It is therefore natural that one may expect Reynolds number effects on the form factor. Such influences have been investigated by several researchers with the aim of establishing empirical corrections to form factor values obtained at low Reynolds numbers (Re). For instance, Min and Kang (2010) used an experimental database to determine that as a ship's scale factor approaches unity, the form factor behaves in two ways. Firstly, Min and Kang (2010) showed the form factor of several ships increases with decreasing scale factor. Secondly, they postulated that a "terminal form factor" exists $(1+k_\infty)$. They defined this "the form factor at the design speed for the full-scale ship". In practice, their results showed that this point is reached around $Re = 10^9$.

The formulation, arrived at by Min and Kang (2010) reads as follows:

$$(1 + k_\infty) / (1 + k) = \tanh(a \times (\log_{10}(Re)^n) \tag{2}$$

where $a = 0.015064$, and $n = 2.6752$.

Similar work was performed earlier by García-Gómez (2000), who used the scale factor as the dependent variable. However, expressing scale effects in terms of the Reynolds number is thought to be more convenient, since it gives an indication of the state of the flow. Specifically, it has been postulated by Min and Kang (2010) that one of the reasons for the Reynolds number dependency, observed by them is due to the fact that at low Re, the flow is not fully turbulent. In full-scale, the flow is turbulent over the vast majority of the hull, in contrast to the model-scale experiment.

With the intent of expanding the understanding of the above-mentioned discrepancies, several researchers have investigated scale effects. Since a ship is tested at a Reynolds number that is several orders of magnitude lower than its full-scale equivalent, work has rightly concentrated on Reynolds number effects. A universal solution to ship resistance, however, is yet to be found. This stems from a variety of sources, including but not limited to:

- The mathematical difficulty associated with wave resistance prediction. The estimation of this component of resistance via potential flow remains an active field of research, with some recent contributions by Yuan et al. (2018), Li et al. (2019), and Bašić et al. (2020) to name but a few.
- The decomposition of ship resistance itself may not be valid for all types of ships and under all circumstances. For instance, the addition of energy saving devices (K. Song et al., 2019), or novel underwater forms may invalidate the form factor approach.
- The necessary assumptions, imposed by definition on the total resistance coefficient's decomposition. For example, the form factor is known to be Reynolds number dependent (Dogrul et al., 2020; Raven et al., 2008; Terziev et al., 2019a; Xiao et al., 2018).

The final point above is best illustrated in graphical form. The ship hull, adopted as a case study in this paper, the KCS, has been subject to a considerable number of form factor assessments. Results from these are depicted in Fig. 1 versus the Reynolds number
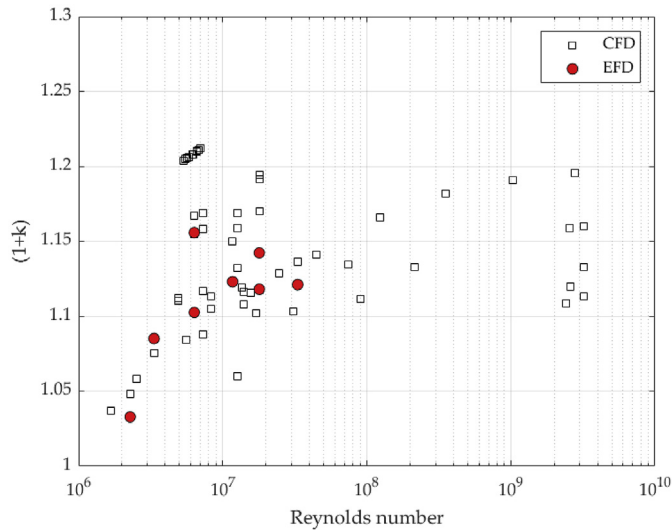
Fig. 1. Form factor values[1] for the KCS, predicted via experimental and computational fluid dynamics (EFD and CFD, respectively).
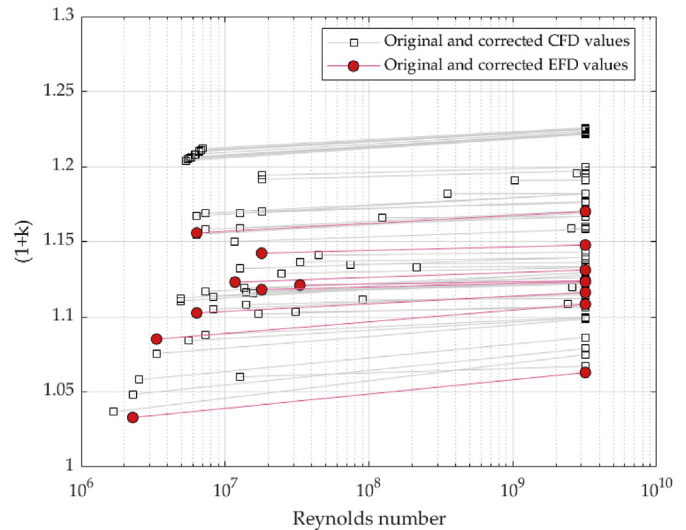

Fig. 2. Computed and measured form factor values. Lines indicate the correction of Min and Kang (2010) to the terminal form factor value.

from each case. The figure features both numerical and experimental work from a wide range of researchers and facilities. It is apparent that the form factor increase, postulated by Min and Kang (2010), is reproduced well. More importantly, Fig. 1 illustrates that academia's concern regarding the assumptions imposed onto the form factor are well placed. There is indeed a strong Reynolds number dependence found both experimentally and numerically.

It is of note that half of the studies used to construct Fig. 1 (Dogrul et al., 2020; Korkmaz et al., 2019a; Lee et al., 2018; Terziev et al., 2019a; Xiao et al., 2018) were published in the two years leading up to the time of writing, although many other studies focusing on different ship forms have also been published in the same period. This is thought to be the case largely thanks to the ITTC's "Combined EFD/CFD" Specialist Committee, which chose the form factor as its first topic upon its creation in 2018, thereby generating academic interest in the subject.

A further conclusion one may draw from Fig. 1 is that form factor estimation near Re $= 10^7$ exhibits significant scatter. However, numerical estimates of (1+k) are characterised by essentially the same degree of ambiguity at Re $> 10^9$, where Min and Kang (2010) placed the terminal form factor (shown in Fig. 2). There are several potential sources for this, associated primarily with the numerical approaches different researchers adopt.

One example such source is turbulence, which can have a profound impact on the flow field (Bhushan et al., 2009; Deng et al., 2004). Indeed, recent work involving the resolution of part of the turbulent kinetic energy spectrum showed good agreement with sea trial data (Pena et al., 2019), indicating this may eventually become the norm. A more complete description of the turbulent flow is not yet thought practical, because the cell number requirements at full-scale are $\mathscr{O}(10^{9\sim12})$ (Liefvendahl and Fureby, 2017). Therefore, the Reynolds averaged approach remains a popular alternative, but there is a need for comparison of different models.

Another instance, resulting in ambiguity is the y^+ strategy. In low Reynolds number flows, the y^+ value may be kept below unity resulting in the description of the turbulent boundary layer down

to the viscous sublayer. Low y^+ meshes are thought to reproduce the flow patterns and forces on a hull with greater consistency, while high y^+ meshes have similarly been validated for the forces. In any case, the approach is typically a function of the users experience and availability of computational resources. On the other hand, imposing similar requirements ($y^+ \leq 1$) to full-scale flows is impractical.

The number of cells, required to achieve y^+ similarity scales as $\lambda^{1.35}$ (Peric, 2019). Therefore, performing a study with $\lambda = 1, 75$, and requiring $y^+ = 1$ at both scale factors, one would have to construct approximately 340 times as many cells for the full-scale simulation than are present for the model ($\lambda = 75$) ship in the wall-normal direction alone. Factoring in a reasonable aspect ratio of the near-wall cells would in all likelihood result in an even greater increase in cell numbers. The alternative, the high y^+ approach, may lead to modelling errors in the flow field at model-scale, but neither approach (high nor low y^+) is fully demonstrated at full-scale. Therefore, despite the numerous recent studies on ship form factors and resistance estimation, several outstanding research questions remain.

The present study intends to contribute to the field by performing a series of double body numerical simulations at different scale factors, while varying the Froude number. Double body simulations feature a symmetry plane in place of the free surface, rendering the wave resistance coefficient (C_W) nil. The definition of the total resistance coefficient (C_T), then becomes:

$$C_T = (1 + k)C_F + \underbrace{C_W}_{=0} \xrightarrow{\quad double\ body \quad} C_T = (1 + k)C_F$$

(3)

To assess the method's sensitivity to turbulence modelling, three widely used approaches are compared: the k-ω model (Wilcox, 2008), the realizable k-ε model (Rodi, 1991; Shih et al., 1995), and the k-ω SST model (Menter, 1994). In an attempt to further supplement the present results, the Reynolds number is also varied by controlling the value of viscosity for constant Froude numbers. This approach has been demonstrated to provide good results by Haase et al. (2016a, 2016b), and is therefore adopted here.

---

[1] Form factor values obtained from the following references: Dogrul et al. (2020), Chen et al. (2016), Korkmaz et al. (2019a,b), Lee et al. (2018), Sukas et al. (2014), Xiao et al. (2018), Yang et al. (2010), Terziev (2019a).

Table 1
Ship particulars.

Quantity	Symbol	Value				Unit
Scale factor	λ	1	31.599	52.667	75	–
Length	L	230	7.279	4.367	3.067	m
Beam	B	32.2	1.019	0.611	0.429	m
Depth	D	19	0.601	0.361	0.253	m
Draught	T	10.8	0.342	0.205	0.144	m
Block coefficient	C_B	0.651	0.651	0.651	0.651	–
Design speed	V	12.350	2.196	1.702	1.426	m/s
Design Froude number	Fr	0.26	0.26	0.26	0.26	–
Design Reynolds number	Re	3.188×10^9	1.794×10^7	8.342×10^6	4.909×10^6	–

Table 2
Reynolds numbers for the linearly scaled simulations.

λ	75	52.667	31.599	1
Fr	Reynolds number			
0.02	3.78×10^5	6.42×10^5	1.32×10^6	2.45×10^8
0.04	7.55×10^5	1.28×10^6	2.64×10^6	4.91×10^8
0.06	1.13×10^6	1.93×10^6	3.95×10^6	7.36×10^8
0.08	1.51×10^6	2.57×10^6	5.27×10^6	9.81×10^8
0.1	1.89×10^6	3.21×10^6	6.59×10^6	1.23×10^9
0.12	2.27×10^6	3.85×10^6	7.91×10^6	1.47×10^9
0.14	2.64×10^6	4.49×10^6	9.22×10^6	1.72×10^9
0.16	3.02×10^6	5.13×10^6	1.05×10^7	1.96×10^9
0.18	3.40×10^6	5.78×10^6	1.19×10^7	2.21×10^9
0.2	3.78×10^6	6.42×10^6	1.32×10^7	2.45×10^9
0.22	4.15×10^6	7.06×10^6	1.45×10^7	2.70×10^9
0.24	4.53×10^6	7.70×10^6	1.58×10^7	2.94×10^9
0.26	4.91×10^6	8.34×10^6	1.71×10^7	3.19×10^9
0.28	5.29×10^6	8.98×10^6	1.84×10^7	3.43×10^9

3. Case studies

To take full advantage of the wealth of data, shown in Fig. 1, the KCS is adopted as a case study. The ship's particulars at the explored scale factors are given in Table 1.

The choice of scale factors, given in Table 1, is rooted in practical considerations. The values of λ, chosen for this assessment reflect experiments performed at different facilities although few experiments report the value of the form factor, which precludes a direct comparison. Nevertheless, the established database of $(1+k)$ values, shown in Fig. 1 is thought to be sufficient for the purposes of this work. The full test matrix includes viscously scaled case studies, which are used to alter the Reynolds number range by two orders of magnitude. The particulars of the viscously scaled simulations are given later in this section.

As mentioned earlier, the Froude number is varied to detect any influences on the form factor. In this study, the value of Fr is spread between 0.02 and 0.28 for each scale factor, with a step of 0.02. This results in 14 speeds at each scale factor and turbulence model. The resulting Reynolds numbers are summarised in Table 2.

The viscously scaled simulations, performed only for λ=75, are used to target the region between Re = 10^7 and Re = 10^8. This is done due to the fact that few studies have performed work in this rage, as shown in Fig. 1. To ensure a representation of both low and high speeds within the above Reynolds number range, four Froude numbers are chosen, representing the lowest (Fr = 0.02, 0.04) and highest speeds (Fr = 0.26, 0.28). Then, to alter the Reynolds number, the viscosity is varied between the default value ($\nu = 8.9986 \times 10^{-7}$) and $\nu = 1.036 \times 10^{-8}$ in 100 equally spaced steps for each of the previously mentioned Froude numbers. This is done to produce a change in the Reynolds number of approximately two orders of magnitude for each Froude number. It should be noted that the ship length is maintained constant throughout all viscously

Table 3
Reynolds number range, covered by the viscously scaled simulations.

Fr	Re	
0.02	Minimum	3.738×10^5
	Maximum	3.248×10^7
0.04	Minimum	7.477×10^5
	Maximum	6.497×10^7
0.26	Minimum	4.860×10^6
	Maximum	4.223×10^8
0.28	Minimum	5.234×10^6
	Maximum	4.548×10^8

scaled simulations (Table 1 may be consulted for $\lambda = 75$), whereas the speed varies according to the previously stated Froude numbers. This results in the Reynolds number ranges, listed in Table 3.

4. Numerical set-up

This section is dedicated to the numerical set-up used to perform all simulations. As stated in the introduction, the commercially available unstructured finite volume solver, Star-CCM+, version 14.02.12 was used throughout. Details of the solver can be accessed in Siemens (2018). To avoid deviating from the core of this paper, only the main details and choices thought to have a palpable impact on the results are given.

The numerical simulations were performed using the segregated flow solver, which solves each momentum equation in turn. Pressure and continuity are linked via a predictor-corrector approach, whereas pressure-velocity coupling is achieved via a SIMPLE algorithm. All simulations were performed using a steady state solver, since the free surface was not modelled in any of the

case studies. This allows for a rapid convergence of the results and reduction in the computational expense. Convergence of the results was monitored via the residuals, which were reduced (at minimum) in the range 10^{-6}–10^{-8} prior to terminating a simulation. The evolution of each case's resistance curve was also monitored to ensure that the flow field had arrived at its converged state prior to ending a simulation.

4.1. Turbulence

Turbulence modelling is considered as one of the main sources of modelling error in CFD. To avoid the excessive effort of solving for the exact turbulent fluctuations in the fluid, it is standard engineering practice to invoke suitable averaging (Durbin and Pettersson Reif, 2011). In other words, one is interested solely in the overall performance, and not in the fluctuations caused by turbulent eddies. Due to the non-linear nature of the governing equations, averaging results in the number of unknowns exceeding the number of equations, rendering the system unclosed. In ship hydrodynamics, there are several well-established approaches to providing closure to the Navier-Stokes equations. The most widely adopted ones, by far, are the two-equation eddy-viscosity models. These require the solution of two additional equations, typically the turbulent kinetic energy (k) and a measure of the decay of turbulent eddies, the dissipation frequency (ω), or dissipation rate (ε).

For the purposes of this study, the k-ω model, the k-ω SST (Shear Stress Transport) and k-ε models were employed. Since it is not the purpose of this work to contribute to the mathematics of turbulence, the underlying relations used to provide closure are omitted. The reader is instead referred to the texts of Durbin and Pettersson Reif (2011), Ferziger and Peric (2002), and Wilcox (2006), and the Star-CCM + user manual for specifics regarding the models' implementation. The aforementioned two-equation eddy-viscosity turbulence models account for the vast majority of research in ship hydrodynamics (Terziev et al., 2019b). Each of the abovementioned turbulence models was applied to each case study, given in Section 3. This is done in an attempt to gauge the turbulence dependence of the problem, and how this is affected by an increase in the Reynolds number of several orders of magnitude.

4.2. Computational domain and boundary conditions

The computational domain was constructed following the guidelines of the ITTC (2014). Specifically, the inlet was placed 1.5 ship lengths upstream of the forward perpendicular, whereas the outlet was set as 2.5 ship lengths downstream of the aft perpendicular. The inlet boundary is prescribed the free stream velocity, set according to the cases given in Table 2. To ensure there is no side and bottom boundary influence on the ship, the corresponding boundaries were placed 2.5 ship lengths from the hull centreline. Here, an inlet boundary condition was imposed. The velocity on these boundaries (bottom and side) is prescribed as the free stream value solely in the negative x direction. This was implemented on all velocity inlet boundaries, thereby approximating an infinite sea. The domain top is placed coincident with the undisturbed free surface, representing the operational draught of the ship (given in Table 1), and set as a symmetry plane. Finally, the ship hull was assigned the no-slip wall condition. The complete arrangement, including the boundary conditions is shown in Fig. 3.

4.3. Mesh generation

The computational mesh was generated within the automatic facilities of Star-CCM+. To begin with, the mesh over the ship's hull was generated. To accomplish this, the prism layer mesher facility was employed. This allows one to construct a high quality near-wall mesh by filling the space between the input surface, in this case the ship hull, and an exploded version of the input with cells of increasing size. To accomplish this, a geometric progression is used with a stretch factor of 1.5. The first cell dimensions are assigned based on the ITTC correlation prediction of the local frictional resistance coefficient as shown in Eq. (4)

$$C_F = \frac{0.075}{(\log_{10}(Re) - 2)^2} = \frac{2\tau_w}{\rho V^2} \tag{4}$$

where τ_w is the shear wall stress, ρ is the fluid density, and V is the free stream velocity. Then, the first layer's width is approximated by:

$$\Delta y = \frac{y^+ \nu}{u_\tau} \tag{5}$$

with $u_\tau = \tau_w / \rho$ being the friction velocity, ν is the viscosity, and y^+ is the non-dimensional distance to the wall. As stated earlier, a high y^+ approach was used throughout. Therefore, values of y^+ between 30 and 300 were used, as shown in Fig. 4.

The core mesh was constructed by requiring that cells at the outer edge of the prism layer mesh were identical to the final layer within the prism layer. Six such cells were created before the
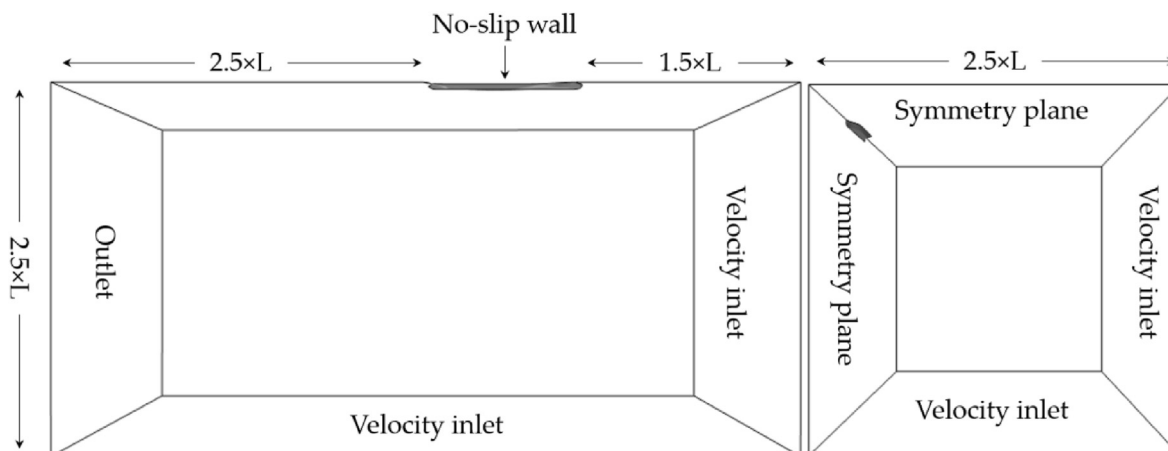
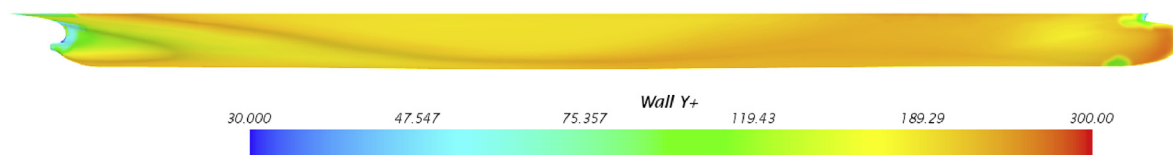**Fig. 3.** Computational domain boundary conditions and dimensions.

Fig. 4. Example y^+ distribution on the hull. Depicted: $\lambda = 31.599$, Fr=0.26.

Table 4
Number of cells.

Scale factor	Number of cells
75	528,223
52.667	1,830,082
32.599	2,790,200
1	9,958,205

characteristic length was allowed to increase. This process was repeated with distance from the hull, until a boundary was reached. The wake of the ship was refined up to a distance of $0.5 \times L$ downstream with cells, equal to those at the edge of the prism layer. The growth rate, mentioned previously was applied for this region as well. The resulting cell numbers can be consulted in Table 4. It should be noted that the cell numbers, given for λ=75 are used for the viscous scaling simulations. The generated grid for $\lambda = 31.599$ is shown in Fig. 5.

4.4. Numerical uncertainty

This section provides an estimate of the numerical uncertainty.

Due to the large number of cases, values are only given for a sample of the results. The remaining uncertainty estimates are depicted graphically to enable a suitable comparison of the results.

Numerical error and uncertainty arise as a result of the discretisation of the continuous form of the governing equations onto discrete nodes. The purpose of a numerical uncertainty estimation exercise is partly to demonstrate that as the characteristic cell size decreases, the predicted numerical error also decreases. For a more in-depth discussion on the subject, the reader is referred to the most recent standard on numerical uncertainty (Freitas, 2020), as well as the ITTC (2008) and ASME (American Society of Mechanical Engineers, 2009) guides.

A numerical uncertainty estimation begins when one obtains solutions on at least three systematically refined or coarsened grids. The solutions form these are denoted f_1, f_2, and f_3 for the fine, medium, and coarse solution, respectively. These solutions should be sufficiently close to the asymptotic range to enable the validity of Richardson Extrapolation (RE) (Roache, 2016), which is the basis of the uncertainty assessment adopted within this study. In this study, the grids are obtained by coarsening the fine grid by a refinement factor, $r = \sqrt{2}$. The method used is known as the Grid Convergence Index (GCI), introduced as a means of uniform reporting of
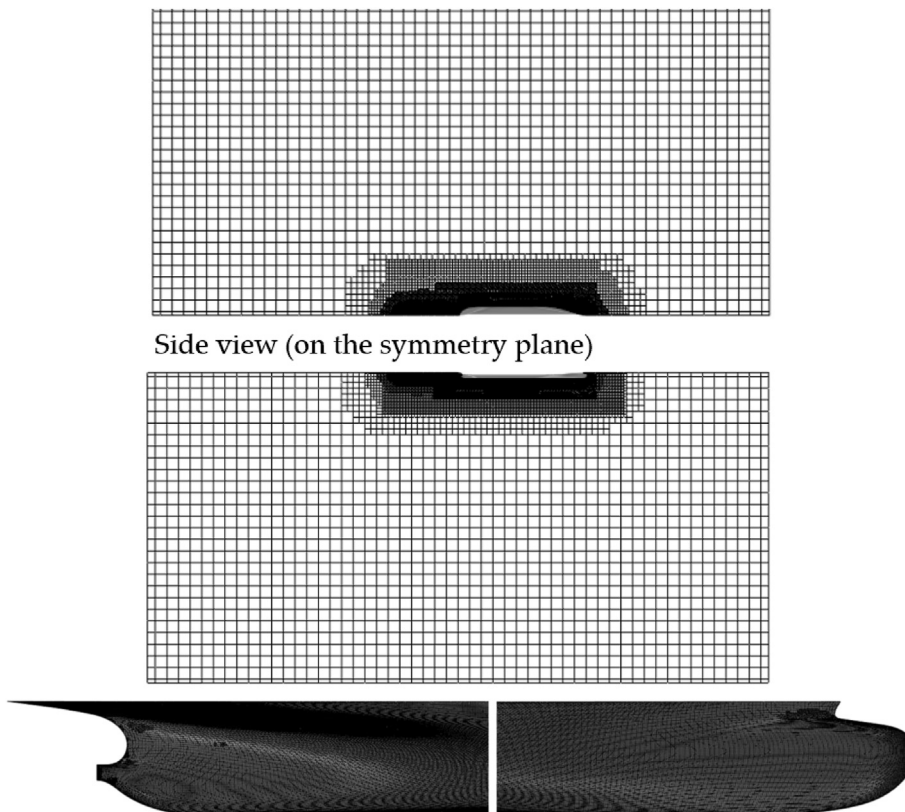

Fig. 5. Top and side view of the mesh for $\lambda = 31.599$, and close-up of the surface mesh on the stern and bow.

uncertainty in numerical studies.

Having obtained the three solutions, mentioned above, it is possible to determine whether the solution converges monotonically, in an oscillatory manner, or if it diverges. This is done based on the convergence ratio, shown in Eq. (6):

$$R = \varepsilon_{21}/\varepsilon_{32} \tag{6}$$

where $\varepsilon_{21} = f_2 - f_1$, and $\varepsilon_{32} = f_3 - f_1$. The three convergence conditions, according to ITTC (2008) are:

1. Monotonic convergence, when $0 < R < 1$
2. Oscillatory convergence, when $R < 0$
3. Divergence, when $R > 1$

Then, according to Celik et al. (2008), the order of accuracy (p) may be predicted by:

$$p = \frac{1}{\ln r}|\ln|\varepsilon_{32}/\varepsilon_{21}| + q(p)| \tag{7}$$

where the function $q(p) = 0$ for uniform refinement, which is the case here, and

$$q(p) = \ln\left(\frac{r_{21}^p - s}{r_{32}^p - s}\right) \tag{8}$$

otherwise. In Eq. (8), $s = sign(\varepsilon_{32}/\varepsilon_{21})$. It should be noted that in the r_{21}, and r_{32} represent the refinement factors of the medium and coarse grid, respectively. Since a uniform refinement factor is used in this study, $r_{21} = r_{32} = r$.

Then, one may predict an extrapolated solution using Eq. (9):

$$f_{ext} = (r_{21}^p f_1 - f_2)/(r_{21}^p - 1) \tag{9}$$

Finally, the fine-grid convergence index reads:

$$GCI = 1.25\left|\frac{f_1 - f_2}{f_1}\right| \Big/ (r_{21}^p - 1) \tag{10}$$

The resulting uncertainty estimates (U) for the full-scale form factors are given in Table 5. In performing the systematic coarsening, the medium (f_2) simulation contained 4,987,483 cells, whereas the coarse (f_3) simulation featured 2,748719 cells.

The assessment, carried out within this section demonstrates that a low numerical uncertainty (below 1%) is achievable over the intermediate to high speed range of Froude numbers at full-scale. However, when the speed is reduced to the lowest value examined as part of this work, the uncertainty tends to increase to 2%–3%. For the purposes of this paper, such levels of numerical uncertainty are considered tolerable.

It should also be noted that in the course of following the steps of the GCI procedure, an extrapolated solution is produced. The extrapolated solution is also referred to as the mesh-independent solution. However, it is not correct to use this value (f_{ext}) as the final solution. This is because it is not possible to demonstrate that such solutions satisfy the laws of conservation.

5. Results and discussion

At the onset of this work, it was stated that one of the objectives was to seek Froude number dependencies on the form factor of a ship. For this reason, the first set of results, presented as part of the present assessment features the linearly scaled simulation results in terms of form factor. These are given against the Froude number, and are grouped by turbulence model, as shown in Fig. 6.

Table 5

Full-scale results from the uncertainty assessment. Note that f_1, f_2, and f_3 are the fine, medium, and coarse values of the form factor (1+k), respectively.

|	Fr	0.02	0.04	0.06	0.08	0.1	0.12	0.14	0.16	0.18	0.2	0.22	0.24	0.26	0.28
	Re	2.45×10^8	4.91×10^8	7.36×10^8	9.81×10^8	1.23×10^9	1.47×10^9	1.72×10^9	1.96×10^9	2.21×10^9	2.45×10^9	2.7×10^9	2.94×10^9	3.19×10^9	3.43×10^9
k-ω	f_1	1.306	1.247	1.229	1.222	1.218	1.216	1.215	1.214	1.213	1.213	1.213	1.213	1.213	1.213
	f_2	1.337	1.265	1.246	1.238	1.234	1.232	1.230	1.230	1.229	1.229	1.228	1.228	1.228	1.228
	f_2	1.291	1.240	1.231	1.229	1.228	1.228	1.229	1.229	1.230	1.230	1.231	1.231	1.232	1.232
	p	2.543	2.629	2.969	3.263	3.572	3.928	4.405	5.428	5.027	4.443	4.173	4.023	3.900	3.798
	f_{ext}	1.285	1.235	1.220	1.214	1.212	1.211	1.211	1.211	1.210	1.209	1.208	1.208	1.207	1.207
	GCI	**2.02%**	**1.18%**	**0.92%**	**0.77%**	**0.65%**	**0.55%**	**0.44%**	**0.28%**	**0.34%**	**0.43%**	**0.48%**	**0.52%**	**0.55%**	**0.57%**
k-ε	f_1	1.170	1.163	1.165	1.168	1.171	1.173	1.175	1.176	1.178	1.179	1.180	1.181	1.182	1.183
	f_2	1.213	1.190	1.189	1.190	1.192	1.194	1.195	1.196	1.197	1.198	1.199	1.200	1.200	1.201
	f_2	1.254	1.210	1.204	1.203	1.204	1.205	1.205	1.206	1.207	1.208	1.209	1.209	1.210	1.210
	p	2.930	3.159	3.261	3.311	3.338	3.354	3.363	3.369	3.374	3.377	3.379	3.380	3.381	3.381
	f_{ext}	1.146	1.149	1.154	1.158	1.161	1.163	1.166	1.167	1.169	1.170	1.171	1.172	1.173	1.174
	GCI	**2.49%**	**1.45%**	**1.20%**	**1.09%**	**1.03%**	**0.98%**	**0.96%**	**0.93%**	**0.92%**	**0.90%**	**0.89%**	**0.88%**	**0.87%**	**0.86%**
k-ω SST	f_1	1.352	1.261	1.216	1.195	1.184	1.177	1.173	1.170	1.167	1.166	1.165	1.164	1.163	1.162
	f_2	1.380	1.281	1.235	1.215	1.204	1.197	1.193	1.190	1.187	1.186	1.184	1.183	1.183	1.182
	f_2	1.277	1.204	1.188	1.182	1.180	1.179	1.179	1.179	1.179	1.179	1.179	1.179	1.180	1.180
	p	1.842	1.884	2.219	2.520	2.760	2.967	3.155	3.333	3.507	3.683	3.868	4.071	4.304	4.594
	f_{ext}	1.320	1.239	1.200	1.181	1.171	1.166	1.162	1.160	1.159	1.158	1.158	1.157	1.157	1.157
	GCI	**2.88%**	**2.09%**	**1.66%**	**1.44%**	**1.29%**	**1.16%**	**1.06%**	**0.97%**	**0.88%**	**0.81%**	**0.74%**	**0.67%**	**0.60%**	**0.53%**
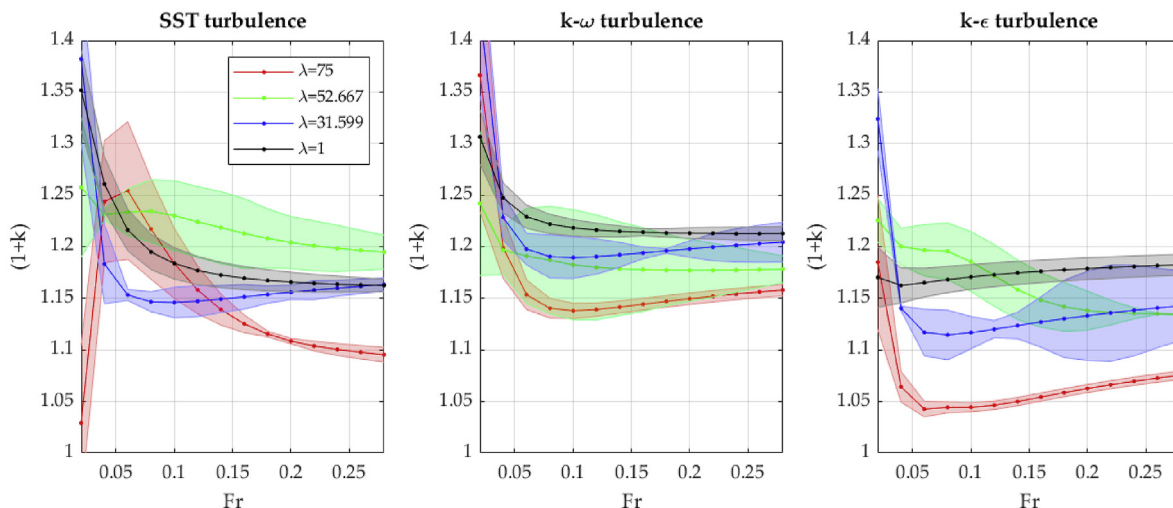
Fig. 6. Computed form factors against Froude number and corresponding numerical uncertainty for each turbulence model and scale factor.

It should be noted that in the present work, the form factor is obtained as the ratio of the total resistance coefficient obtained by CFD and the C_F value calculated using Eq. (1) (the ITTC correlation line).

In Fig. 6, the shaded area, surrounding each curve is used to represent the uncertainty, computed as stated in section 4.4. Clearly, the uncertainty for each turbulence model, scale factor and speed differ from each other. This is a testament to the turbulence dependence of the problem examined herein. It also highlights that depending on one's choice regarding turbulence model, the results may be palpably different. For instance, should one prefer the SST model and a scale factor of $\lambda = 52.667$ for the highest examined speed, the results in terms of form factor would be in the vicinity of $(1 + k)_{SST,\lambda=52.667} = 1.195$, with a reasonable numerical uncertainty of $U_{SST,\lambda=52.667} = 1.37\%$. On the other hand, if the k-ε model were to be employed for the same scale factor, the form factor would be $(1 + k)_{k-\varepsilon,\lambda=52.667} = 1.134$, with an uncertainty of $U_{k-\varepsilon,\lambda=52.667} = 0.12\%$. In other words, a 5.4% absolute difference in $(1+k)$.

The above example is a 'best case scenario', in which the analyst is interested solely in the form factor achieved at the highest speed. However, in the event where lower speeds are investigated, the results differ by a greater margin. For example, the k-ω model reproduces a characteristic shape in the form factor curve over the Froude number range examined. That is, high initial values, which decrease abruptly in the range up to Fr = 0.1, following which the form factor exhibits little change with further speed increase. On the other hand, the SST and k-ε models do not reproduce this behaviour for all scale factors. Specifically, the SST turbulence model predicts that the form factor is $(1 + k)_{SST,\lambda=75} = 1.029$ with $U_{SST,\lambda=75} = 11.88\%$, whereas the k-ε models - $(1 + k)_{k-\varepsilon,\lambda=75} = 1.185$ and $U_{k-\varepsilon,\lambda=75} = 11.01\%$. This amounts to an absolute difference of 15.16%, which is higher than the uncertainty bounds of either method. The overall pattern, which is produced in Fig. 6 suggests that the present RANS approach is challenged to a greater extent at the very low speed limit (Fr = 0.02−0.06), where the numerical uncertainty is highest in the majority of cases.

Since the form factor is multiplied by the frictional resistance confident within the ITTC performance prediction method approach, it is important to state the consequences of a significant deviation in $(1+k)$. The frictional resistance may account for the majority of the total resistance for some ships (S. Song et al., 2019; Tezdogan et al., 2016a). Therefore, a significant change, or epistemic uncertainty, associated with the form factor is detrimental to ship

design. This is because the naval architect would ideally seek an accurate estimate for the total resistance, which determines the characteristics of the power plant of a ship for a certain speed (Tezdogan et al., 2016b). In the event where a design exhibits unfavourably high resistance, alterations may be necessary.

Several datapoints, particularly those at low speeds in Fig. 6, exhibit considerable numerical uncertainty. Nevertheless, as shown in Fig. 7, the majority of predictions exhibit an acceptable level of numerical uncertainty, between 0% and 2%, with few exceptions past 6%. The low levels of uncertainty, however, do not allow the identification of specific directions or trends over all turbulence models. That is to say, the predicted form factors exhibit a weak dependence on the Froude number, based on the data presented jointly in Figs. 6 and 7, factoring in numerical uncertainty. At the lowest Froude numbers examined, the CFD method predicts a significant variation of the form factor, when compared to the highest speed. However, the numerical uncertainty is typically elevated in the former region, thereby making concrete arguments
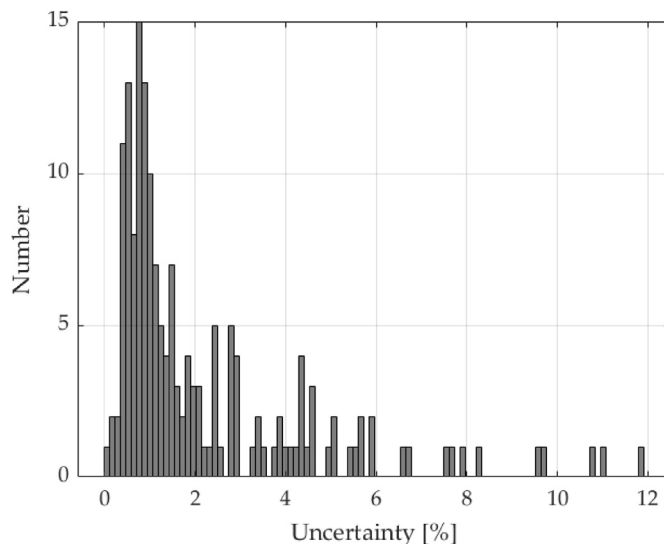

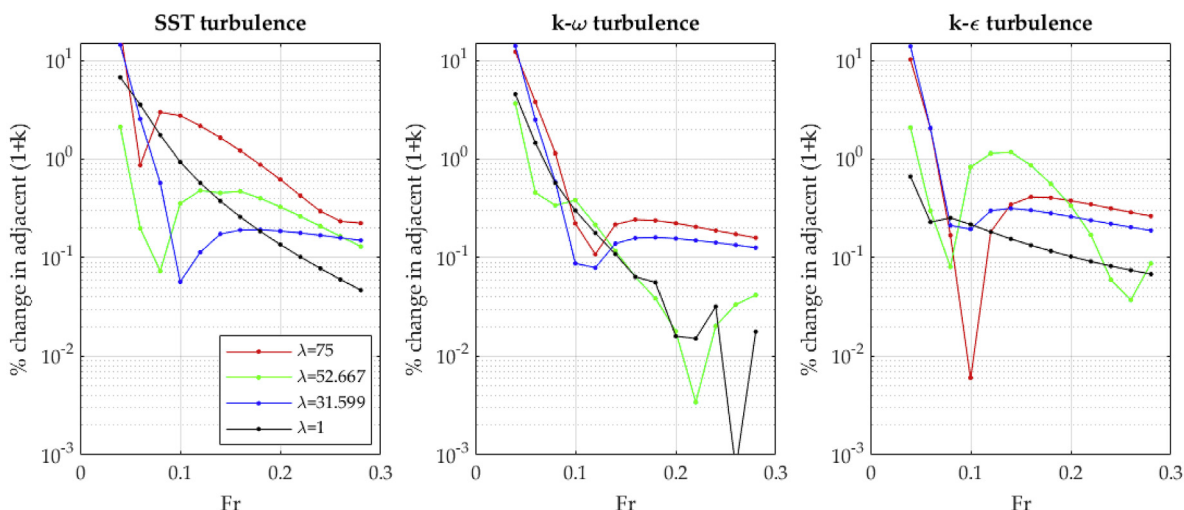**Fig. 7.** Distribution of the numerical uncertainty for the ship's form factor.

Fig. 8. Absolute difference between $(1+k)$ predicted at adjacent Froude numbers for all turbulence models and scale factors.

difficult. This is compounded by the small difference over the Froude number range for each scale factor and turbulence model at higher speeds, although some variation is observed.

The SST turbulence model at $\lambda = 75$ exhibits a change of approximately 21% between the lowest and second lowest speeds (Fr = 0.02, $(1+k) = 1.029$, and Fr = 0.04, where $(1+k) = 1.244$). Following this abrupt change, the predicted form factors vary by up to 3%, until Fr = 0.16, after which the change in adjacent $(1+k)$ values is below 1%. The same model shows a similar trend at $\lambda = 31.599$, with an initial change of 14.38%. Following this, the form factors do not vary more than 2.5% at Fr = 0.06. Moreover, the $(1+k)$ values vary less than 0.5% thereafter. On the other hand, the SST model for $\lambda = 52.667$ and $\lambda = 1$, the maximum change between adjacent form factors is 2.1% and 6.7%, respectively, both of which occur for the lowest speed. In the intermediate and high speed range, the change is in all cases below 1%.

The k-ω model shows abrupt changes in the form factor for the two lowest speeds only at $\lambda = 75$, 31.599, where the difference between Fr = 0.02 and Fr = 0.04 is 12.26% and 14.02%, respectively. The k-ε model also behaves in a similar manner to the k-ω model, with 10.2% and 13.87% difference for the two lowest speeds at the scale factors $\lambda = 75$ and $\lambda = 31.599$, respectively. These results are graphically summarised in Fig. 8, where it can be seen that as the intermediate Froude number range is reached, the RANS model tends to predict a considerably smaller influence of the Fr on the form factor.

On the other hand, the absolute differences found between the three lowest and the highest speed ($100 \times |(1+k)_{Fr=0.02} - (1+k)_{Fr=0.28}| / (1+k)_{Fr=0.28}$, for example) for each scale factor and turbulence model are given in Table 6. Here, it is apparent that in most cases, the relative difference between the two pairs of Froude numbers decreases rapidly with increasing speed.

Such differences in the form factor are likely to be absorbed within the correlation allowance, and are not considered highly influential. However, the dependence on turbulence for each form factor is significantly higher, indicating that depending on the case this may not be fully captured within the correlation allowance.

The numerically predicted form factor of a ship is predominantly influenced by the location of the frictional resistance coefficient with respect to the ITTC line's value for a particular Reynolds number. If the friction, as predicted by CFD is lower than the ITTC line, then the form factor will also be low. On the other hand, if the ITTC line is exceeded, the form factor will show greater values. Since double body simulations are performed within the present assessment, the frictional resistance coefficient accounts for the vast majority of the total, and therefore has the greatest influence on the value of the form factor. This is depicted in Fig. 9 for all scale factors and turbulence models, respectively.

In Fig. 9, the resistance coefficients are given against Reynolds number. The numerical uncertainty is also included via error bars to give the reader a visual estimate of the confidence interval involved

Table 6
Absolute relative difference between the lowest (Fr = 0.02, 0.04, 0.06) and highest speed, examined in this study (Fr = 0.28).

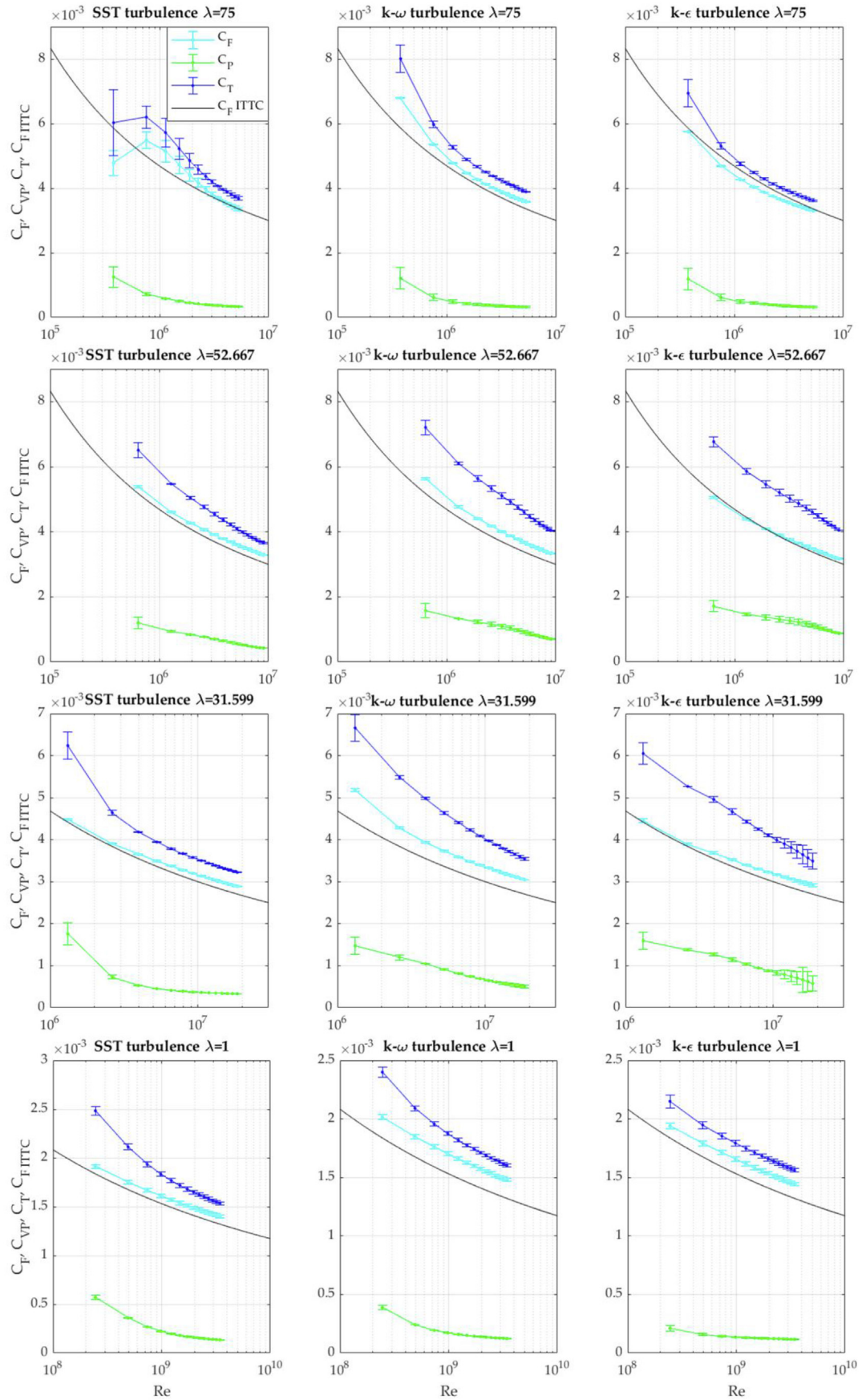| Fr	λ	75	52.667	31.599	1	Mean
0.02 and 0.28	SST	6.04%	5.27%	18.80%	16.28%	11.60%
	k-ω	17.99%	5.41%	18.61%	7.72%	12.43%
	k-ε	10.18%	8.08%	15.85%	1.03%	8.79%
Mean		11.40%	6.25%	17.75%	8.34%	**10.94%**
0.04 and 0.28	SST	13.55%	3.04%	1.71%	8.47%	6.69%
	k-ω	3.53%	1.55%	1.98%	2.83%	2.47%
	k-ε	1.05%	5.84%	0.22%	1.69%	2.20%
Mean		6.04%	3.48%	1.30%	4.33%	**3.79%**
0.06 and 0.28	SST	14.54%	3.24%	0.87%	4.63%	5.82%
	k-ω	0.38%	1.09%	0.56%	1.34%	0.84%
	k-ε	3.07%	5.52%	2.27%	1.47%	3.08%
Mean		6.00%	3.28%	1.23%	2.48%	**3.25%**

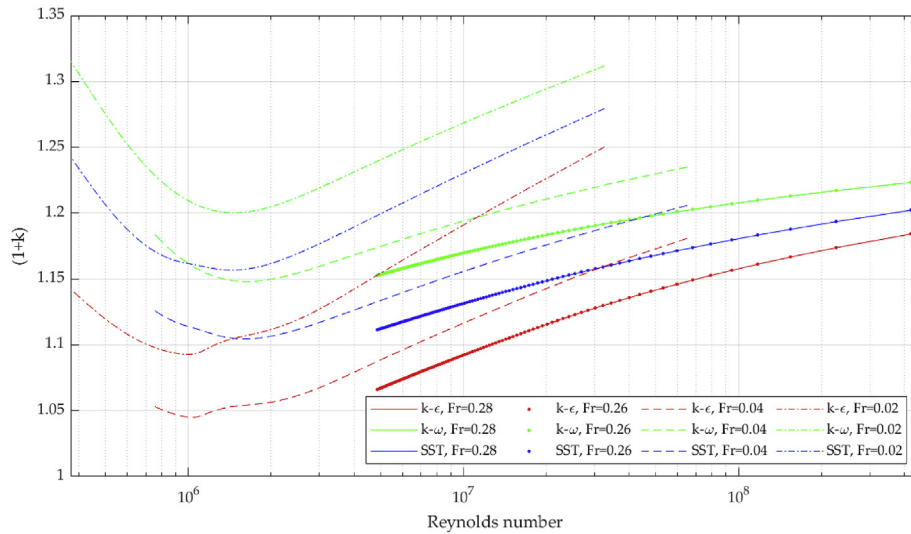**Fig. 9.** Resistance coefficients obtained for all scale factors and turbulence models.

Fig. 10. Viscously scaled simulation's form factor predictions.

in each prediction. This approach is adopted due to the large number of predictions. The data used to create all figures within this work is available to download freely via the University of Strathclyde repository (https://doi.org/10.15129/177ff072-cd23-4762-9492-2f495a4879d3).

Fig. 9 suggests that the ITTC line provides good agreement with the CFD-based frictional resistance coefficients. Overall, all except $\lambda = 75$ for the k-ε model and low speeds of $\lambda = 52.667$ and $\lambda = 31.599$ provide values for C_F higher than the ITTC line. In the case of for $\lambda = 75$, the SST turbulence model predicts that the frictional resistance coefficient increases abruptly at the low Re range, following which it traces out the ITTC line.

With the exception of the full-scale results, the viscous pressure resistance coefficient is responsible for a considerable numerical uncertainty, carried into the total resistance coefficient, and thereby into the form factor prediction. This may be deduced by the
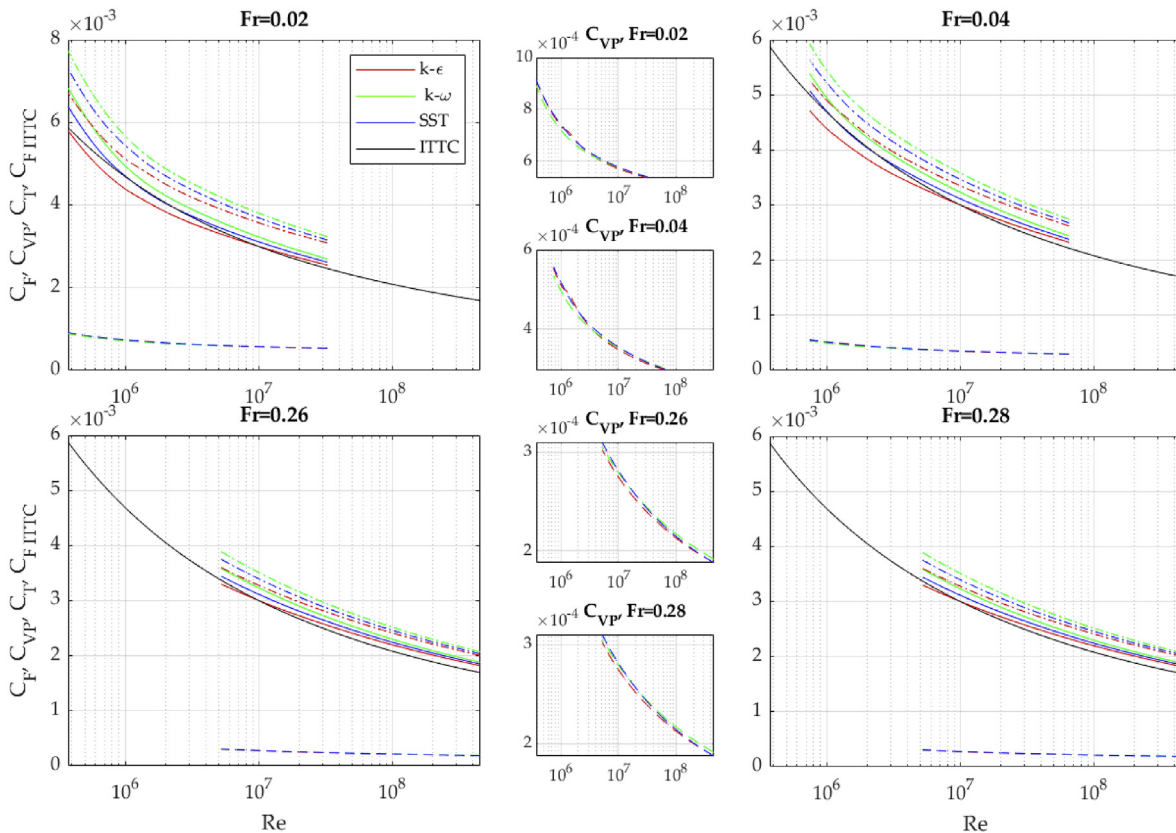
Fig. 11. Resistance coefficients, obtained via the viscously scaled simulations. Solid lines represent C_F, dashed lines are used for C_{VP}, and broken lines for C_T.

fact that the locations of increased numerical uncertainty in the viscous pressure resistance coefficient always coincide with the total resistance coefficient's elevated numerical uncertainty. This is true despite the fact that the aforementioned component of the total accounts for a small fraction of the total. A similar conclusion was reached by Farkas et al. (2019) in their work. This paper therefore confirms their results.

The viscous pressure resistance coefficient exhibits little turbulence dependence overall, with one notable exception, specifically, the SST turbulence model at low speed $\lambda = 31.599$. The viscous pressure resistance coefficient is characterised by a rather sharp decline, not exhibited by the other two turbulence models, which show an approximately linear trend over the depicted Reynolds numbers.

At this stage, the viscously scaled simulation results are introduced, beginning with the form factor predictions, depicted in Fig. 10. As mentioned in section 3, only the lowest and highest speeds are examined using this approach (specifically, Fr = 0.02, 0.04, 0.26, and 0.28). An immediate conclusion, drawn from Fig. 10 is that as the speed increases, the numerical method predicts a significant decrease in the form factor, in agreement with the majority of predictions in Fig. 6. The difference over the Reynolds number range, i.e. Re-dependence, is comparable to the turbulence dependence, exhibited by the different methods.

As the Froude number is increased form Fr = 0.02 to Fr = 0.04, the curve, representing the form factor approaches the high-speed predictions. This is consistently predicted across all turbulence models. Fig. 10 suggests that a Froude number exists, past which the form factor is essentially speed-independent, and is only influenced by the Reynolds number. This may be deduced by the fact that the predictions for Fr = 0.26 and Fr = 0.28 are essentially identical for all turbulence models.

The influence of turbulence dependence is seen to decrease over the Reynolds number. For example, for the smallest Reynolds number (Re = 5.234×10^6), forming part of the viscously scaled simulations' range at Fr = 0.28, the form factor predictions are $(1 + k)^{Re=4.548 \times 10^8}_{k-\varepsilon, Fr=0.28} = 1.069$ and $(1 + k)^{Re=4.548 \times 10^8}_{k-\omega, Fr=0.28} = 1.154$, for the k-ε and k-ω models, respectively. This results in an absolute difference of 7.415%, which decreases to 3.156% at the end of the Reynolds number scale (Re = 4.548×10^8), where $(1 + k)^{Re=4.548 \times 10^8}_{k-\varepsilon, Fr=0.28} = 1.185$ and $(1 + k)^{Re=4.548 \times 10^8}_{k-\omega, Fr=0.28} = 1.224$.

The pattern of diminishing turbulence dependence is observed for all four examined Froude numbers. This suggests that as the Reynolds number increases, turbulence modelling plays an increasingly reduced role. Such an observation is consistent with
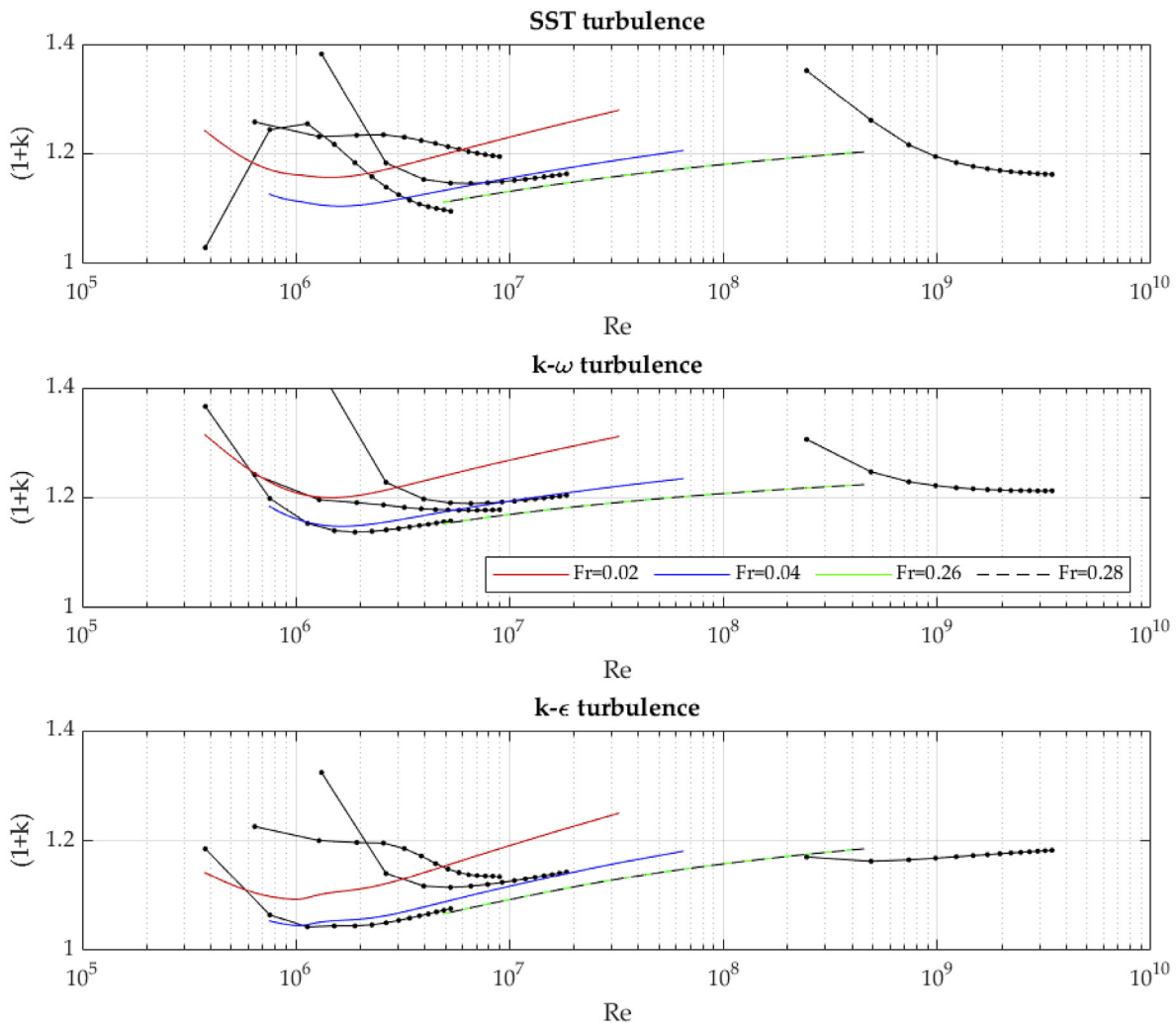

Fig. 12. Comparison of all form factors, computed in this study. Coloured lines represent the viscously scaled simulations, whereas the lines with markers represent the linearly scaled simulations.
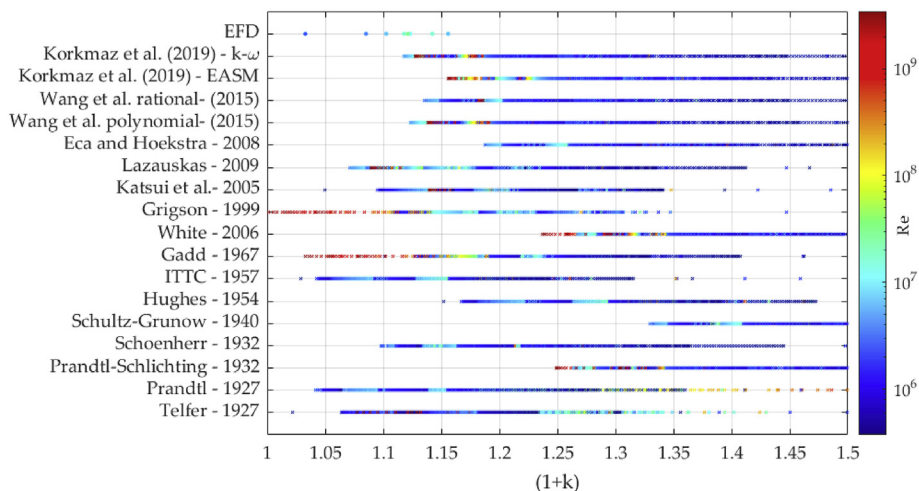
Fig. 13. Form factor values predicted via a variety of methods.

the fact that in the Navier-Stokes equations, when written in non-dimensional form, the viscous term is expressed as 1/Re (for high Reynolds number flows). This observation also explains the fact that at full-scale, a ship's boundary layer is thinner than at model-scale.

Next, the resistance coefficients, obtained via the viscously scaled simulations are given. These can be seen in Fig. 11 for all Froude and Reynolds numbers investigated in this paper. In Fig. 11, both axes' range are maintained constant to enable a better comparison of the performance of the viscously scaled method against the ITTC line. Here, it is apparent that deviations from the ITTC line, particularly below it, are mostly present for low Froude numbers. This is consistent with the previously observed fact that at low speeds, the RANS approach is challenged to a greater extent than at intermediate or high speeds. Although the numerical uncertainty assessment is not performed for the viscously scaled simulations, it can be reasonably expected that similar confidence intervals would be observed here as was the case for the linearly scaled simulations.

Fig. 11 also contains a comparison of the viscous pressure resistance coefficient. Here, the ordinate is varied to demonstrate that turbulence modelling has little influence on this particular parameter. The viscous pressure resistance coefficient's scale effect is also noticeable, which is characterised by a noticeable decrease over the Reynolds number range.

To enable a comparison of the different approaches, adopted in this study (viscous scaling and linear scaling), Fig. 12 contains the form factor predictions using both methods. As was the case earlier, the form factor predictions a grouped in terms of turbulence model and are depicted over the entire range of examined Reynolds numbers. Fig. 12 suggests that the different methods exhibit some disagreement in the specific value of the form factor, but the trend of general increase in form factor with Reynolds number from 10^6 to 10^9 is reproduced everywhere. The full-scale results show a decline with changing Froude number (in the range $10^8 < Re < 10^{10}$). There is also a well-established dependence on the turbulence model. The k-ε closure exhibits the lowest form factors, whereas the k-ω — the highest, with the SST model located between these. Such a behaviour of the SST model could be forecast, based on the fact that this particular closure is a blend of the other two. It is therefore not surprising that predictions made by the SST model would tend to lie between the k-ε and k-ω predictions.

Another way in which one ought to consider the results is by varying the friction line used. For instance, in recent years, a

number of friction lines have emerged, constructed by fitting equations to frictional resistance coefficients obtained from numerical simulations of flat plates. For instance, such studies were performed by Eca and Hoekstra (2008), Korkmaz et al. (2019b), and Wang et al. (2015). Alternatively, there are a variety of approaches, available to express C_F as a function of the Reynolds number without the use of numerical methods. Thus, one may calculate the form factor without using the ITTC correlation line, which takes into account the longitudinal and transverse curvature of the ship. To demonstrate the influence of different approaches, Fig. 13 contains 17 selected methods (Eca and Hoekstra, 2008; Gadd, 1967; Grigson, 1999; Hughes, 1954; Katsui et al., 2005; Korkmaz et al., 2019b; Lazauskas, 2009; Prandtl, 1925; Schoenherr, 1932; Schultz-Grunow, 1941; Telfer, 1927; Wang et al., 2015; White, 2006). It should be noted that the figure also contains additional details regarding the numerical approach used to obtain the relevant friction lines, such as turbulence model. Furthermore, the experimentally determined form factors, shown in Fig. 1 are included for comparison in Fig. 13.

Fig. 13 demonstrates the importance of the choice of friction line, that is, if the correlation allowance is addressed by some other method. The results from Fig. 13 suggest that Grigson's (1999) and Gadd's (1967) lines predict form factors at full-scale Reynolds number in close agreement with the experimental values given in Fig. 1 using the total (double body) resistance coefficients, computed in this study. Additionally, the recent line of Korkmaz et al. (2019b), obtained using the k-ω model shows similar results, with a cluster of high Reynolds number form factors at the lower end of the range. However, this may not necessarily be taken as a measure of success, since the scale effect of the form factor may cause the results to vary considerably using the abovementioned friction lines, depending on the ship type.

To enable a better understanding of the tendency of each line in terms of form factor predictions using the present data as input (from Figs. 13), Fig. 14 is constructed to depict the distribution of each prediction method alongside the experimental data.

Fig. 14 suggests that using some friction lines may be better than others. However, it is important to keep in mind that there are no guarantees regarding the robustness of the total resistance coefficients, predicted within this study. This is the case in part because the double body approach was used throughout, which does not capture the full spectrum of physical phenomena of the problem at hand. While one may have reasonable confidence in the
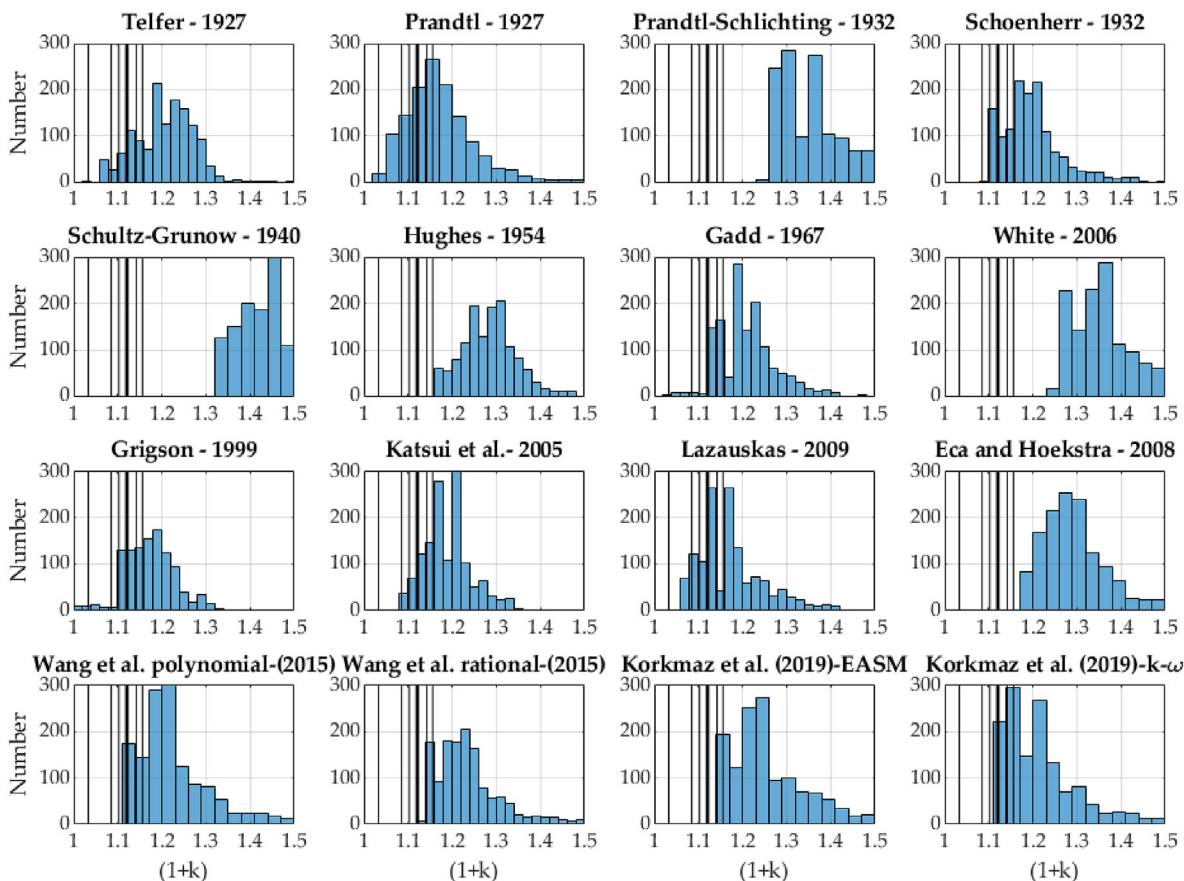
Fig. 14. Distribution of predicted form factors using each method. Vertical lines indicate experimental values.

form factors presented herein due to their relative agreement with experimentally obtained $(1+k)$ values, this would not be the case for a novel ship form. This highlights the need for research in the area of scale effects and resistance extrapolation. Such a study was performed by Farkas et al. (2018), where advantages and disadvantages of extrapolation methods and the impact of four turbulence models are shown.

6. Conclusion

This study set out to investigate Froude number dependencies on the form factor of a ship by using a RANS approach. Three widely used turbulence models, the k-ω model, the k-ω SST model, and k-ε model were used on the KCS hull at four scale factors ($\lambda = 75$, 52.667, 31.599, 1), which were applied to 14 Froude numbers. To further supplement the test matrix, the viscous scaling approach was utilised, where the Reynolds number is varied not by a change in the linear dimension of the ship, but rather a change in the viscosity of the surrounding fluid.

The results showed a strong dependence on the Froude number in the very low speed range (Fr = 0.02, 0.04, 0.06), where abrupt changes in the prediction of the form factor across all turbulence models and almost all scale factors was observed. The maximum difference between any two form factors, predicted at adjacent speeds was found to be approximately 20.9%, which was recorded for the SST turbulence model at $\lambda = 75$ and Fr = 0.02, 0.04. In all cases, the difference between form factors, computed at adjacent Froude numbers, as well as the difference between the lowest and

highest speeds showed a decline when increasing the lowest speed. In most cases, this difference began around 10–20%, reaching values below 1% difference past the intermediate range of Froude numbers.

In terms of numerical uncertainty, the majority of results showed a grid dependence below 2%, with few outliers past 5%. These outliers were found to be exclusively stemming from the cases where the Froude number is in the range Fr = 0.02–0.06. This behaviour of the RANS model suggests a difficulty and stronger grid dependence at the very low Froude number range, which quickly diminishes with increasing speed.

The ship's frictional resistance coefficient was shown to trace out the ITTC line in the intermediate and high speed range, but some differences were observed in the low speed range. Differences between the numerical frictional resistance coefficients and ITTC correlation line are likely related to the RANS model's performance at low speeds, discussed previously. The Froude and Reynolds numbers where the numerical uncertainty of the viscous pressure coefficient was greatest coincided with the largest numerical uncertainty of the total resistance coefficient. On the other hand, the frictional resistance coefficient was shown to carry a relatively small uncertainty in the vast majority of cases. This indicated that the viscous pressure resistance coefficient has a major influence in numerical prediction of the total resistance, despite its small magnitude in the double body simulations. For all scale factors and turbulence models, the viscous pressure coefficient was shown to decline monotonically.

The viscous scaling approach largely confirmed the observations

made for the linearly scaled simulations. Namely, the low speed range was associated with a considerable scale effect, which rapidly reduces with increasing Froude number. In fact, the viscously scaled simulations suggested no Froude number effect between $Fr = 0.26$ and $Fr = 0.28$. Over the entire range of Reynolds numbers explored with the viscously scaled approach, the frictional resistance coefficient was in good agreement with the ITTC line, while the viscous pressure resistance showed the abovementioned decline with increasing Reynolds number.

Further research is necessary to fully capture and determine the nature of the scale effect on the form factor, both in terms of Froude and Reynolds number dependencies. An experimental study in geosim form, performed in a single facility would be most beneficial to the field, particularly if wake measurements are taken at each scale factor. Shallow and restricted waters are require further attention, although some studies have recently examined scale effects in such cases, further work would be highly beneficial.

Declaration of competing interest

The authors declare that they have no known competing financial interests or personal relationships that could have appeared to influence the work reported in this paper.

Acknowledgements

References

ASME (American Society of Mechanical Engineers), 2009. Standard for Verification and Validation in Computational Fluid Dynamics and Heat Transfer - ASME V&V 20-2009. ASME International.

Bašić, J., Blagojević, B., Andrun, M., 2020. Improved estimation of ship wave-making resistance. Ocean. Eng. 200, 107079. https://doi.org/10.1016/j.oceaneng.2020.107079.

Bhushan, S., Xing, T., Carrica, P., Stern, F., 2009. Model- and full-scale URANS simulations of athena resistance, powering, seakeeping, and 5415 maneuvering. J. Ship Res. 53, 179—198.

Celik, I.B., Ghia, U., Roache, P.J., Freitas, C., 2008. Procedure for estimation and reporting of uncertainty due to discretization in CFD applications. J. Fluid Eng. 130, 078001 https://doi.org/10.1115/1.2960953.

Chen, X., Zhu, R., Ma, C., Fan, J., 2016. Computations of linear and nonlinear ship waves by higher-order boundary element method. Ocean. Eng. 114, 142—153. https://doi.org/10.1016/j.oceaneng.2016.01.016.

Deng, G., Duvigneau, R., Queutey, P., Visonneau, M., 2004. Assessment of turbulence models for ship flow at full scale. In: Comp. Mech., WCCM VI. Beijing, China.

Dogrul, A., Song, S., Demirel, Y.K., 2020. Scale effect on ship resistance components and form factor. Ocean. Eng. 209, 107428. https://doi.org/10.1016/j.oceaneng.2020.107428.

Durbin, P.A., Pettersson Reif, B.A., 2011. Statistical Theory and Modelling for Turbulent Flow, second ed. Wiley.

Eca, L., Hoekstra, M., 2008. The numerical friction line. J. Mar. Sci. Technol. 13, 328—345. https://doi.org/10.1007/s00773-008-0018-1.

Farkas, A., Degiuli, N., Martić, I., 2018. Assessment of hydrodynamic characteristics of a full-scale ship at different draughts. Ocean. Eng. 156, 135—152. https://doi.org/10.1016/j.oceaneng.2018.03.002.

Farkas, A., Degiuli, N., Martić, I., Dejhalla, R., 2019. Numerical and experimental assessment of nominal wake for a bulk carrier. J. Mar. Sci. Technol. 24, 1092—1104. https://doi.org/10.1007/s00773-018-0609-4.

Ferziger, J.H., Peric, M., 2002. Computational Methods for Fluid Dynamics. Springer. https://doi.org/10.1016/S0898-1221(03)90046-0.

Freitas, C.J., 2020. Standards and methods for verification, validation, and uncertainty assessments in modeling and simulation. J. Verif. Valid. Uncertain. Quantif. 5, 1—9. https://doi.org/10.1115/1.4047274.

Froude, W., 1874. Report to the Lords Commissioners of the Admiralty on Experiments for the Determination of the Frictional Resistance of Water on a Surface, under Various Conditions, Performed at Chelston Cross, under the Authority of Their Lordships.

Gadd, G.E., 1967. A new turbulent friction formulation based on a reappraisal of Hughes' results. Trans. RINA 109, 109—511.

García-Gómez, A., 2000. On the form factor scale effect. Ocean. Eng. 27, 97—109. https://doi.org/10.1016/S0029-8018(98)00042-0.

Gotman, A., 2007. A history of ship resistance evaluation. J. Ocean Technol. 2, 74—96.

Gotman, A., 2002. Study of michell's integral and influence of viscosity and ship hull form on wave resistance. Ocean. Eng. Int. 6, 74—115.

Grigson, C.W.B., 1999. A planar friction algorithm and its use in analysing hull resistance. Trans. RINA.

Haase, M., Davidson, G., Binns, J., Thomas, G., Bose, N., 2016a. Full-scale resistance prediction in finite waters: a study using computational fluid dynamics simulations, model test experiments and sea trial measurements. Proc. Inst. Mech. Eng. Part M J. Eng. Marit. Environ. 231, 316—328. https://doi.org/10.1177/1475090216642467.

Haase, M., Zurcher, K., Davidson, G., Binns, J.R., Thomas, G., Bose, N., 2016b. Novel CFD-based full-scale resistance prediction for large medium-speed catamarans. Ocean. Eng. 111, 198—208. https://doi.org/10.1016/j.oceaneng.2015.10.018.

Havelock, T., 1908. The Propagation of Groups of Waves in Dispersive Media, with Aplication to Waves on Water Produced by a Travelling Disturbance 422—451. https://doi.org/10.1098/rspa.1933.0074.

Hughes, G., 1954. Friction and form resistance in turbulent flow and a proposed formulation for use in model and ship correlation. Trans. Inst. Nav. Arch. 96.

ITTC, 2017. Recommended procedures 1978 ITTC performance prediction method, 4th revision, 7.5 — 02 03 — 01.4. In: 28th Int Towing Tank Conf.

ITTC, 2014. ITTC — recommended procedures and guidelines - practical guidelines for ship CFD applications. 7.5-03-02-03 (revision 01). In: ITTC — Recomm. Proced. Guidel. 19.

ITTC, 2008. Uncertainty analysis in CFD verification and validation methodology and procedures. In: 25th ITTC 2008, Resist. Comm. 12.

Katsui, T., Asai, H., Himeno, Y., Tahara, Y., 2005. The proposal of a new friction line. In: Fifth Osaka Colloquium on Advanced CFD Applications to Ship Flow and Hull Form Design, Osaka, Japan.

Korkmaz, K.B., Werner, S., Bensow, R., 2019a. Investigations for CFD based form factor methods. 22nd numer. In: Towing Tank Symp. (NuTTS 2019), Tomar, Port.

Korkmaz, K.B., Werner, S., Bensow, R.E., 2019b. Numerical friction lines for CFD based form factor determination. In: VIII International Conference on Computational Methods in Marine Engineering MARINE 2019.

Kouh, J.S., Chen, Y.J., Chau, S.W., 2009. Numerical study on scale effect of form factor. Ocean. Eng. 36, 403—413. https://doi.org/10.1016/j.oceaneng.2009.01.011.

Lazauskas, L.V., 2009. Resistance, Wave-Making and Wave-Decay of Thin Ships, with Emphasis on the Effects of Viscosity.

Lee, Y.G., Ha, Y.J., Lee, S.H., Kim, S.H., 2018. A study on the estimation method of the form factor for a full-scale ship. Brodogradnja 69, 71—87. https://doi.org/10.21278/brod69105.

Li, Y., Smeltzer, B.K., Ellingsen, S., 2019. Transient wave resistance upon a real shear current. Eur. J. Mech. B Fluid 73, 180—192. https://doi.org/10.1016/j.euromechflu.2017.08.012.

Liefvendahl, M., Fureby, C., 2017. Grid requirements for LES of ship hydrodynamics in model and full scale. Ocean. Eng. 143, 259—268. https://doi.org/10.1016/j.oceaneng.2017.07.055.

Menter, F.R., 1994. Two-equation eddy-viscosity turbulence models for engineering applications. AIAA J. 32, 1598—1605. https://doi.org/10.2514/3.12149.

Min, K.-S., Kang, S.-H., 2010. Study on the form factor and full-scale ship resistance. J. Mar. Sci. Technol. 15, 108—118. https://doi.org/10.1007/s00773-009-0077-y.

Pena, B., Muk-Pavic, E., Ponkratov, D., 2019. Achieving a high accuracy numerical simulations of the flow around a full scale ship. In: Proceedings of the International Conference on Offshore Mechanics and Arctic Engineering - OMAE, pp. 1—10. https://doi.org/10.1115/OMAE2019-95769.

Peric, M., 2019. White paper: full-scale simulation for marine design. Siemens White Pap 1—14.

Prandtl, L., 1925. Report on the investigation of developed turbulence, Translation of " Bericht über Untersuchungen zur ausgebildeten Turbulenz. Z. Angew. Math. Mech. 5 (2). April 1925.

Raven, H.C., van der Ploeg, A., Starke, A.R., Eca, L., 2008. Towards a CFD-based prediction of ship performance—progress in predicting full-scale resistance and scale effects. Int. J. Marit. Eng. 150.

Roache, P.J., 2016. Verification and validation in fluids engineering: some current issues. J. Fluid Eng. 138, 101205. https://doi.org/10.1115/1.4033979.

Rodi, W., 1991. Experience with two-layer models combining the k-epsilon model with a one-equation model near the wall. In: 29th Aerospace Sciences Meeting. https://doi.org/10.2514/6.1991-216.

Schoenherr, K., 1932. Resistance of flat surfaces moving through a fluid. Trans. - Soc. Nav. Archit. Mar. Eng. 40, 279—313.

Schultz-Grunow, F., 1941. New Frictional Resistance Law for Smooth Plates.

Shih, T.H., Liou, W.W., Shabbir, A., Yang, Z., Zhu, J., 1995. A new k-ε eddy viscosity model for high Reynolds number turbulent flows. Comput. Fluids 24, 227—238. https://doi.org/10.1016/0045-7930(94)00032-T.

Siemens, 2018. Star-CCM+ User Guide Version 13.04.

Song, K., Guo, C., Wang, C., Sun, C., Li, P., Zhong, R., 2019a. Experimental and numerical study on the scale effect of stern flap on ship resistance and flow field. Ships Offshore Struct. 1–17. https://doi.org/10.1080/17445302.2019.1697091, 0.

Song, S., Demirel, Y.K., Atlar, M., 2019b. An investigation into the effect of biofouling on the ship hydrodynamic characteristics using CFD. Ocean. Eng. 175, 122–137. https://doi.org/10.1016/j.oceaneng.2019.01.056.

Sukas, O.F., Kinaci, O.K., Bal, S., 2014. Computation of total resistance of ships and a submarine by a RANSE based CFD. In: INT-NAM, Istanbul, Turkey. https://doi.org/10.13140/2.1.3013.6329.

Telfer, E.V., 1927. Ship resistance similarity. Trans. R. Inst. Nav. Archit. 69, 174–190.

Terziev, M., Tezdogan, T., Incecik, A., 2019a. A geosim analysis of ship resistance decomposition and scale effects with the aid of CFD. Appl. Ocean Res. 92 https://doi.org/10.1016/j.apor.2019.101930.

Terziev, M., Tezdogan, T., Incecik, A., 2019b. Application of eddy-viscosity turbulence models to problems in ship hydrodynamics. Ships Offshore Struct. 1–24. https://doi.org/10.1080/17445302.2019.1661625.

Tezdogan, T., Incecik, A., Turan, O., 2016a. Full-scale unsteady RANS simulations of vertical ship motions in shallow water. Ocean. Eng. 123, 131–145. https://doi.org/10.1016/j.oceaneng.2016.06.047.

Tezdogan, T., Incecik, A., Turan, O., Kellett, P., 2016b. Assessing the impact of a slow steaming approach on reducing the fuel consumption of a containership advancing in head seas. Transp. Res. Procedia 14, 1659–1668. https://doi.org/

10.1016/j.trpro.2016.05.131.

Tuck, E.O., Lazauskas, L.V., 2008. Drag on a ship and Michell's integral. In: 22nd Int. Congress of Theoretical and Applied Mechanics, Adelaide, South Australia, August.

Wang, Z.Z., Xiong, Y., Shi, L.P., Liu, Z.H., 2015. A numerical flat plate friction line and its application. J. Hydrodyn. 27, 383–393. https://doi.org/10.1016/S1001-6058(15)60496-6.

White, F., 2006. Viscous Fluid Flow, third ed. McGraw-Hill.

Wilcox, D.C., 2008. Formulation of the k-w turbulence model revisited. AIAA J. 46, 2823–2838. https://doi.org/10.2514/1.36541.

Wilcox, D.C., 2006. Turbulence Modeling for CFD, third ed. Transportation Research Record. DCW Industries. https://doi.org/10.1016/j.aqpro.2013.07.003.

Xiao, Z., Guo, L., Fend, D., Lai, S., Hu, Z., 2018. Numerical study on the scale effects of the ship resistance and form factor. In: 2018 IEEE 8th Int. Conf. Underw. Syst. Technol. Theory Appl., pp. 1–6.

Yang, H.-U., Kim, B.-N., Yoo, J.-H., Kim, W.-J., 2010. Wake comparison between model and full scale ships using CFD. J. Soc. Nav. Archit. Korea 47, 150–162. https://doi.org/10.3744/snak.2010.47.2.150.

Yuan, Z.M., Zhang, X., Ji, C.Y., Jia, L., Wang, H., Incecik, A., 2018. Side wall effects on ship model testing in a towing tank. Ocean. Eng. 147, 447–457. https://doi.org/10.1016/j.oceaneng.2017.10.042.